THE JOURNAL OF PHYSICAL CHEMISTRY B

Article

pubs.acs.org/JPCB

Low-Temperature Carbonization and More Effective Degradation of Carbohydrates Induced by Ferric Trichloride

Juan Xia,[†] Le Xin Song,*[,†,‡] and Zheng Dang[†]

[†]Department of Chemistry, University of Science and Technology of China, Hefei 230026, People's Republic of China

[‡]State Key Laboratory of Coordination Chemistry, Nanjing University, Nanjing 210093, People's Republic of China

Supporting Information

ABSTRACT: The present work is devoted to an attempt to understand the effect of an inorganic salt such as ferric trichloride ($FeCl_3$) on the carbonization and degradation of carbohydrates such as β-cyclodextrin (CD), amylose, and cellulose. Our data revealed two important observations. First, the presence of $FeCl_3$ led to the occurrence of a low carbonization temperature of 373 K. This is a rare phenomenon, in which carbonization improvement is present even if a small amount of $FeCl_3$ was added. Experimental results had provided evidence for the fact that a redox process was started during the low-temperature carbonization of β-CD, causing the reduction of $FeCl_3$ to ferrous chloride ($FeCl_2$) by carbon materials formed in the carbonization process in air. However, the reduction process of $FeCl_3$ produced the in situ composite nanomaterial of Fe−$FeCl_2$ combination in nitrogen. Second, a molecule−ion interaction emerged between $FeCl_3$ and the carbohydrates in aqueous solution, resulting in a more effective degradation of the carbohydrates. Moreover, our results demonstrated that $FeCl_3$ played the role of a catalyst during the degradation of the carbohydrates in solution. We believe that the current work not only has a significant potential application in disposal of waste carbohydrates but also could be helpful in many fields such as environmental protection, biomass energy development, and inorganic composite nanomaterials.

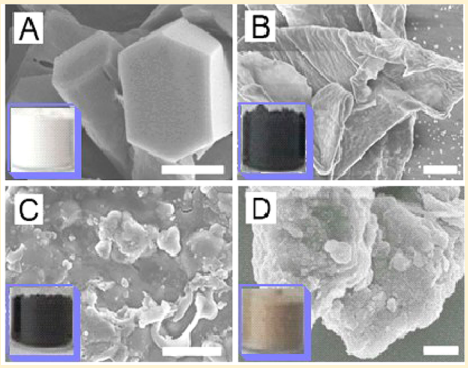

INTRODUCTION

In recent years, there has been more and more particular emphasis on the problem of a shortage of energy resources and refuse treatment.[1−8] At present, the exploitation of biomass energy is one of the hottest topics. Carbohydrates, as one important biomass energy, are one of the renewable energy resources available from food residues, straws, leaves, and so forth.[4−8] Therefore, effective degradation of carbohydrates into useful materials is playing a more and more important role not only in reducing environmental risk but also in developing and utilizing biomass energy.[9−13]

As we know, the degradation of carbohydrates has been extensively studied in recent years.[14−18] There are two main methods widely used; one is based on inorganic acid/alkali degradation,[19−22] and the other is enzyme degradation.[23−27] β-Cyclodextrin (CD) is an important cyclic carbohydrate.[28−42] Recently, we found that the degradation process of β-CD was significantly associated with the presence of inorganic salts.[43−48] A typical example was that the adduct interaction between copper chloride and β-CD led to the degradation of the adducted β-CD that was earlier than that of free β-CD.[49] This phenomenon has aroused our curiosity to investigate whether and how the carbonization process of β-CD is involved in the ion-induced degradation.

In the present work, we tried to answer this question by investigating the thermal behavior of β-CD, amylose, and cellulose in the presence of ferric trichloride ($FeCl_3$) both in aqueous solution and in the solid state. Our experiments yielded a striking result; at the lower drying temperature of 373 K, the β-CD in the presence of $FeCl_3$ was carbonized in its entirety at the time. To the best of our knowledge, no one has reported that such a carbonization phenomenon could occur in cyclic carbohydrates at so low a temperature.

Originally, we speculated that the reason for this may be ascribe to the fact that the increase of acidity in the medium due to the release of hydrogen ions driven by the hydrolysis of $FeCl_3$ had an effect on the degradation of β-CD into small molecules. Indeed, in an acid medium, many carbohydrates could hydrolyze to produce monosaccharides,[50−53] which could easily be carbonized at 373 K. To test this hypothesis, controlled experiments were performed to evaluate the effect of acidity on the hydrolysis of β-CD. Our results showed that the acid conditions (pH, 2.0) caused no significant carbonization of β-CD possibly because β-CD was hydrolyzed only slightly at this pH. It means that $FeCl_3$ has played a significant role in promoting the degradation and carbonization of β-CD. More importantly, the promoting role played by $FeCl_3$ takes effect even at a small amount of addition.

A mechanism was then proposed to explain the promoting role, in which $FeCl_3$ acts as a catalyst, leading to the more

Received: March 30, 2012
Revised: June 11, 2012
Published: June 12, 2012

effective degradation of β-CD into reducing sugars in solution. Subsequently, the sugars are easily carbonized at a lower temperature. Several experiments were conducted to support the mechanism, including X-ray diffraction (XRD), Fourier transform infrared (FTIR), cyclic voltammogram (CV), electrospray ionization mass spectrometry (ESI-MS), and ultraviolet visible (UV−vis) absorption. At last, the effect of $FeCl_3$ on the carbonization of amylose and cellulose was also explored.

In short, the low-temperature carbonization and more effective degradation of carbohydrates induced by $FeCl_3$ provide a novel potential approach to meeting the challenge of the treatment and use of more and more waste carbohydrates that current society produces. It is hoped that this study will be of some use in environmental protection and biomass energy development.

EXPERIMENTAL SECTION

Materials. β-CD was purchased from Shanghai Chemical Reagent Company. Amylose, cellulose, and hydrochloric acid (HCl) were products of Sinopharm Chemical Reagent Co., Ltd. $FeCl_3·6H_2O$ was obtained from Guangdong Xilong Chemical Reagent Company and used as received without further purification. All other chemicals were of general purpose reagent grade, unless otherwise stated.

Preparation of Solid Samples. An aqueous solution (100 mL, adjusted to pH 2.0 with HCl) containing $FeCl_3·6H_2O$ (0.54 g, 2.00×10^{-2} mol·dm^{-3}) and β-CD (2.27 g, 2.00×10^{-2} mol·dm^{-3}) was stirred for 4 h at 333 K; then, water was removed from the solution by rotary evaporation below 323 K. An intimate mixture was obtained after drying for a week at room temperature. Futher, a black solid ($\mathbf{M_1}$) was obtained when the intimate mixture was dried in a drying chamber at 373 K for 2 h. $\mathbf{M_2}$ (black solid) and $\mathbf{M_3}$ (brown solid) were prepared with the same method but with 2.00×10^{-3} and 0 mol·dm^{-3} initial concentrations of $FeCl_3·6H_2O$, respectively. $\mathbf{M_4}$ (black solid) and $\mathbf{M_5}$ (brown solid) were prepared when β-CD was replaced by amylose (2.27 g) using the same method at 2.00×10^{-2} and 0 mol·dm^{-3} concentrations of $FeCl_3·6H_2O$, respectively. $\mathbf{M_6}$ (black solid) and $\mathbf{M_7}$ (brown solid) were prepared when β-CD was replaced by cellulose (2.27 g) using the same method with 2.00×10^{-2} and 0 mol·dm^{-3} concentrations of $FeCl_3·6H_2O$, respectively.

$\mathbf{M_1}$ was dissolved in 50 mL of ethanol in a round-bottomed flask. The undissolved material was mechanically removed by a centrifuge filter to give a yellow−green filtrate. The ethanol in the filtate was removed by rotary evaporation below 323 K, and then, a yellow−green solid ($\mathbf{M_8}$) was obtained after drying in a vacuum over phosphorus pentoxide at 373 K for 2 h. Finally, all of the solid samples were kept in a vacuum desiccator until further use.

Instruments and Methods. XRD analyses of $\mathbf{M_1}$−$\mathbf{M_8}$ were carried out in a Philips X'Pert Pro X-ray diffractometer. Samples were irradiated with monochromatized Cu Kα and analyzed in the 2θ range from 5 to 90°. The tube voltage and current were 40 kV and 40 mA, respectively. Crystal morphologies of β-CD and $\mathbf{M_1}$−$\mathbf{M_3}$ were characterized using a Supra 40 field emission scanning electron microscope (FE-SEM) operated at 5 kV.

FTIR spectra of β-CD and $\mathbf{M_1}$−$\mathbf{M_3}$ were recorded in a Bruker Equinox 55 spectrometer with KBr pellets in the range of 4000−400 cm^{-1} with a resolution of 0.5 cm^{-1}. Raman spectra of β-CD and $\mathbf{M_1}$−$\mathbf{M_3}$ were measured in the range of 200−1800 cm^{-1} with a LABRAM-HR confocal laser microRaman spectrometer with a resolution of 0.6 cm^{-1} at room temperature.

X-ray photoelectron spectroscopy (XPS) of $\mathbf{M_8}$ and the in situ composite nanomaterial of Fe−$FeCl_2$ were recorded at Photoemission Station of National Synchrotron Radiation Laboratory of Hefei with a VG Scienta R3000 electron energy analyzer using Al Kα radiation (1486.6 eV) in ultrahigh vacuum (2.00×10^{-9} Torr) at room temperature. The energy resolution of the instrument was 0.16 eV. The C1s peak (284.8 eV) was used as the internal standard for binding energy calibration.

Thermogravimetric/differential thermogravimetric (TG/DTG) analyses of β-CD, amylose, cellulose, and $\mathbf{M_1}$, $\mathbf{M_4}$, and $\mathbf{M_6}$ were done on a Shimadzu TGA-50 thermogravimetric analyzer at a heating rate of 10.0 K·min^{-1} under a nitrogen atmosphere with a gas flow of 25 mL·min^{-1}. The in situ composite nanomaterial of Fe and $FeCl_2$ was obtained by sintering the intimate mixture of $FeCl_3·6H_2O$ (0.54 g, 2.00×10^{-2} mol·dm^{-3}) and β-CD (2.27 g, 2.00×10^{-2} mol·dm^{-3}) in a tube furnace (Nabertherm, M7/11, with a program controller) under a nitrogen atmosphere at 373 K for 2 h. The sample then continued to heat from 373 to 873 K at the heating rate of 5 K·min^{-1} and was kept at 873 K for 15 min.

CV curves of solutions were obtained using a LK2005 Electrochemical Workstation (LANLIKE, Tianjin, China). The solutions (pH, 2.0) of $FeCl_3·6H_2O$ (2.00×10^{-2} mol·dm^{-3}) in the absence and presence of β-CD (2.00×10^{-2} mol·dm^{-3}) were first stirred for 4 h at 333 K and then cooled to room temperature before use. The glassy carbon disk electrode (GCE) was used as the working electrode, with a platinum wire as the counter electrode and a saturated calomel electrode (SCE) as the reference electrode.

ESI-MS was carried out on an LTQ linear ion trap mass spectrometer (Thermo Fisher Scientific). Before the experiment began, the solutions of β-CD (2.27 g, 2.00×10^{-2} mol·dm^{-3}) after treatment without and with $FeCl_3$ were acidified to pH 2 with HCl. The aqueous solution (10 mL, pH 2.0) containing $FeCl_3·6H_2O$ (0.54 g, 2.00×10^{-2} mol·dm^{-3}) and β-CD was stirred for 4 h at 333 K. Subsequently, the solution was desalted with hydrogen ion-exchange resin (Amberlite IR-120 H^+). At last, the acidic solution was diluted to 1.13×10^{-5} mol·dm^{-3}. The acidic solutions of amylose (2.27 g) after treatment without and with $FeCl_3$ were obtained using the same method. The solutions prepared were injected via a syringe pump at a rate of 1−3 μL·min^{-1}. The nebulizer gas was nitrogen, and the ion spray voltage was 5 kV. Data for each sample were acquired for 2 min in the mass range of m/z = 150−2000.

UV−vis absorption spectra of solutions were taken on a Shimadzu UV 2401-(PC) spectrometer over the wavelength range from 190 to 800 nm, using quartz cells with a 1 cm optical path at room temperature. The solutions (10 mL, adjusted to pH 2.0 with HCl) of $FeCl_3·6H_2O$ (0.54 g, 2.00×10^{-2} mol·dm^{-3}) in the absence and presence of β-CD (2.27 g, 2.00×10^{-2} mol·dm^{-3}) were stirred for 4 h at 333 K and diluted 100-fold with the deionized water before use.

RESULTS AND DISCUSSION

Low-Temperature Carbonization of β-CD Induced by $FeCl_3$. Figure 1 shows XRD patterns of dried β-CD (373 K) and $\mathbf{M_1}$−$\mathbf{M_3}$. We notice that the dried β-CD shows sharp peaks at 2θ angles of 11.2, 13.0, 13.7, 18.5, 19.3, and 24.3°. However, at the same drying temperature, $\mathbf{M_1}$, $\mathbf{M_2}$, and $\mathbf{M_3}$ present one

dx.doi.org/10.1021/jp303041v | J. Phys. Chem. B 2012, 116, 7635−7643

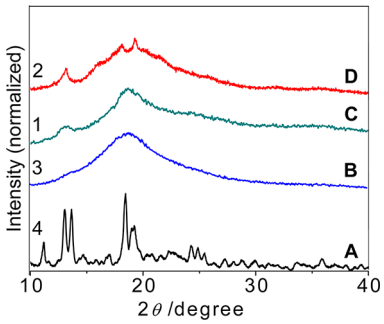

Figure 1. XRD patterns of the dried β-CD (A), $\mathbf{M_1}$ (B), $\mathbf{M_2}$ (C), and $\mathbf{M_3}$ (D). The relative signal intensity was normalized to the intensity of the peak at 18.5° in curve A.

(centered at 18.6°, broad), two (centered at 13.1 and 18.6°, broad), and three peaks (13.2, 18.1, and 19.3°), respectively. This obervation reflects that both the acid conditions and the presence of $FeCl_3$ make the crystallinity of β-CD poorer, and the effect of the latter seems to be larger than that of the former. Moreover, this effect of $FeCl_3$ is dependent on its concentration. Further, the appearance of the broad peak centered at 18.6° due to packing of adjacent carbon chains[54−58] suggests that many of the β-CD molecules have been carbonized at such a temperature (373 K). Results of Raman analysis demonstrate this point.

Figure 2 presents Raman spectra of dried β-CD and the $\mathbf{M_1}$ series materials. Clearly, the bands of the β-CD in curve A,

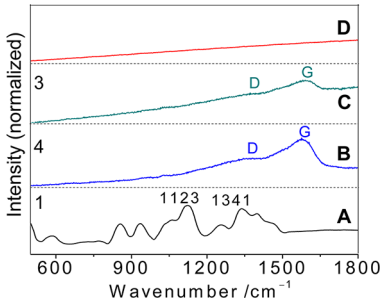

Figure 2. Raman spectra of the dried β-CD (A), $\mathbf{M_1}$ (B), $\mathbf{M_2}$ (C), and $\mathbf{M_3}$ (D). The relative signal intensity was normalized to the intensity of the peak at 1123 cm^{-1} in curve A.

including two strong bands at 1123 (vibrations of C−H bonds in plane)[59,60] and 1341 cm^{-1} (C−C vibration mode),[61] disappear in the $\mathbf{M_1}$ series materials. Instead, two new Raman bands centered at 1380 (D band) and 1575 cm^{-1} (G band) are generated in $\mathbf{M_1}$ and $\mathbf{M_2}$, attributed to disordered and ordered graphitic carbon materials, respectively.[62−67] In addition, the intensity ratios of the D band to the G band are determined to be 0.34 and 0.43 in curves B and C, respectively, showing a high level of graphitic structure. This provides evidence for the analysis of XRD patterns. It is worthy of note that no signals of carbon materials are detected in $\mathbf{M_3}$, suggesting that the high acidity itself cannot cause the occurrence of significant carbonization of β-CD. This is a rare example of the carbonization behavior of a cyclic polysaccharide at such a temperature. It implies that $FeCl_3$ plays a crucial role in facilitating the rupture of 1,4-glycosidic bonds of β-CD. This interpretation is supported by FTIR spectra in Figure 3.

From Figure 3A, the dried β-CD displays characteristic vibration bands at 1080 and 1030 cm^{-1} (shown in the green

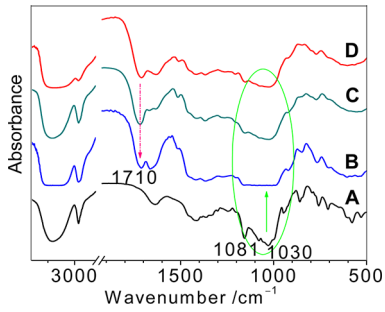

Figure 3. FTIR spectra of the dried β-CD (A), $\mathbf{M_1}$ (B), $\mathbf{M_2}$ (C), and $\mathbf{M_3}$ (D).

circle), corresponding to the stretch vibration of C−O−C linkages of glucose units.[68−71] They still exist in the $\mathbf{M_2}$ and $\mathbf{M_3}$ but completely disappear in $\mathbf{M_1}$, as indicated by the green arrow in Figure 3. This finding reveals that a higher concentration of $FeCl_3$ exerts a larger effect on the cleavage of C−O−C linkages. Additionally, a new vibration band at 1710 cm^{-1} appears in all three $\mathbf{M_1}$ series materials (indicated by the red arrow), which can be assigned to the carbonyl stretching mode of carboxylic groups.[72,73] Therefore, we infer that the β-CD molecules in the $\mathbf{M_1}$ series materials are not only carbonized to a different extent but are also partially degraded into organic molecules such as carboxylic acids. The former originates from the drying process at such a low temperature, and the latter is a result of a reaction in an aqueous medium, both of which may be associated with the significant interaction between $FeCl_3$ and β-CD.

Besides this, we performed another control experiment under neutral conditions (pH 7.0). We noticed that the product obtained without $FeCl_3$ using the same preparation method exhibits almost the same diffraction pattern as the dried β-CD in Figure 1A, having peaks at 2θ angles of 11.2, 13.0, 18.5, and 24.3°.[74] Moreover, the product is white in appearance.[74] These results, together with Figure 1D and Figure 4D, further demonstrate the effect of the acidity.

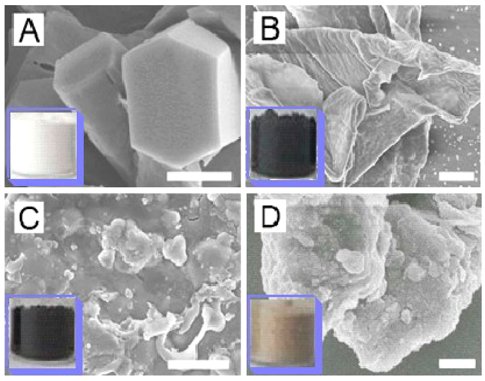

Figure 4. Photographs and FE-SEM images of the dried β-CD (A), $\mathbf{M_1}$ (B), $\mathbf{M_2}$ (C), and $\mathbf{M_3}$ (D). Scale bar = 1 μm.

The larger effect of $FeCl_3$ relative to the high acidity can be easily seen from the color difference of the associated samples. The bottom left of Figure 4 shows the photographs of the dried β-CD (white), $\mathbf{M_1}$ (black), $\mathbf{M_2}$ (black), and $\mathbf{M_3}$ (brown). Also, it gives us a hint that the carbonization of β-CD is present even if a small amount of $FeCl_3$ is added. FE-SEM images of the figure illustrate a change in surface features of the materials. The single crystal of the β-CD is shaped like a hexagonal

dx.doi.org/10.1021/jp303041v | J. Phys. Chem. B 2012, 116, 7635−7643

prism,[75−77] roughly 1−2 μm in side length and 1−3 μm in height. However, the particles of $\mathbf{M_1}$ look like a thin pancake with a thickness of about 100 nm, while the crystals of $\mathbf{M_2}$ and $\mathbf{M_3}$ have the shape of an irregular sand grain.

Taking all of the results together, it is concluded that the presence of $FeCl_3$ leads to low-temperature carbonization (373 K) of β-CD. Importantly, even a low concentration of $FeCl_3$ used in the present study does give a satisfactory result. This has a significant potential application in treating carbohydrate wastes. Here, a probable explanation on the low-temperature carbonization is proposed as follows. High acidity and especially the interaction between $FeCl_3$ and β-CD facilitate the rupture of 1,4-glycosidic bonds of β-CD, causing the structural breakdown of the D-glucopyranose rings of β-CD molecules into fragments such as sugar units and small organic molecules or ions.[78−82] Furthermore, the carbonization of the fragments is easier than that of β-CD molecules. In scientific inference, what we need to know is the nature of such an interaction. Further research has been done to solve the problem.

Reduction of $FeCl_3$ to Ferrous Chloride ($FeCl_2$). Figure 5 shows the XRD pattern of $\mathbf{M_8}$. Two sets of characteristic

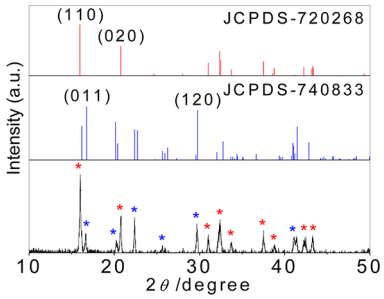

Figure 5. The XRD pattern of $\mathbf{M_8}$.

peaks are observed. The first diffraction peaks at 2θ angles of 15.9, 20.8, 31.1, 32.4, and 33.7° (marked by red asterisks), corresponding to (110), (020), (111), ($\bar{2}$01), and (130), respectively, are indexed to the monoclinic crystal system of $FeCl_2{\cdot}2H_2O$ (JCPDS 72-0268) with lattice constants a = 0.74, b = 0.86, and c = 0.36 nm.[83,84] The second diffraction peaks at 16.7, 20.3, 22.3, 29.7, and 41.1° (marked by blue asterisks), corresponding to (011), (110), (102), (120), and (130), respectively, are in good agreement with monoclinic crystal structure of $FeCl_2{\cdot}4H_2O$ (JCPDS 74-0833) with lattice constants a = 5.91, b = 7.17, and c = 8.44 Å.[85,86] There is no peak corresponding to $FeCl_3$ or its hydrates,[87,88] strongly implying that the $FeCl_3$ in the original solution has been completely reduced to $FeCl_2$ in $\mathbf{M_1}$.

XPS experiments provide evidence for the analysis mentioned above. As shown in Figure 6, the commercial $FeCl_2$ shows the binding energies of Fe(II) $2p_{3/2}$ and $2p_{1/2}$ at 711.1 and 724.0 eV and their satellite peaks at 715.8 and 729.9 eV, respectively.[89−91] However, the binding energies of the Fe(II) in the $\mathbf{M_8}$ shift to 710.5 and 723.6 eV and the satellite peaks nearly disappear. At the same time, the binding energies of Cl $2p_{3/2}$ and $2p_{1/2}$ have shifted from 198.6 and 200.2 eV in the $FeCl_2$ to 198.2 and 199.8 eV in the $\mathbf{M_8}$. The synchronous decrease (indicated by black arrows) in the binding energies of Fe and Cl suggests that the Fe−Cl ionic bonds are weakened because of the interaction with the fragments from the degradation of β-CD as well as residual β-CD, leading to an

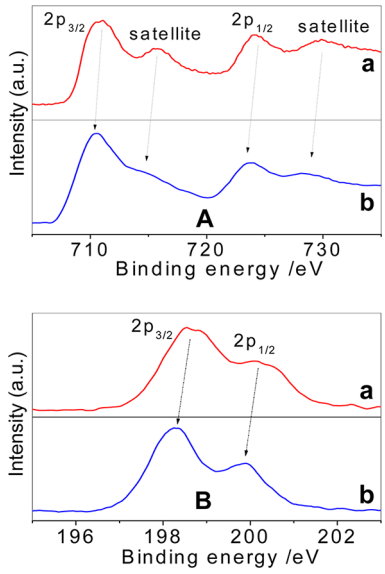

Figure 6. (A) XPS-(Fe_{2p}) and (B) XPS-(Cl_{2p}) spectra of commercial $FeCl_2$ (a) and $\mathbf{M_8}$ (b).

increase in the electron densities of Fe and Cl ions. It should be noted that no splitting is present for the Fe 2p peaks. The result, together with the fact that no other signal of Fe(III) is detected in XRD analysis, indicates that the Fe exists in the form of Fe(II) in the two solid samples ($\mathbf{M_1}$ and $\mathbf{M_8}$). This leads us to ask an obvious question, how is the reduction of Fe^{3+} to Fe^{2+} accomplished? Hence, further investigations are required to determine which of the two processes (the degradation process in aqueous solution and the carbonization process in the solid state) is involved in the reduction reaction.

In order to determine the valence state of Fe, we present CV diagrams (Figure 7) of $FeCl_3{\cdot}6H_2O$ (2.00×10^{-2} mol·dm^{-3},

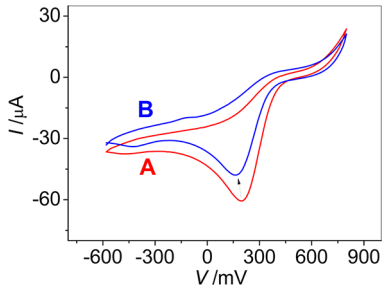

Figure 7. CV curves of the solutions (pH, 2.0) of $FeCl_3{\cdot}6H_2O$ (2.00×10^{-2} mol·dm^{-3}) in the absence (A) and presence (B) of β-CD (2.00×10^{-2} mol·dm^{-3}).

pH 2.0) and the solution (pH 2.0) containing $FeCl_3{\cdot}6H_2O$ (2.00×10^{-2} mol·dm^{-3}) and β-CD (2.00×10^{-2} mol·dm^{-3}) in the range of −600−800 mV in water at room temperature with a voltage sweep rate of 50 mV·s^{-1}. Obviously, the solution containing $FeCl_3{\cdot}6H_2O$ and β-CD shows an extremely similar CV pattern to the commercial $FeCl_3$ solution. In the two samples, only one reduction peak is observed, and it is assigned to Fe(III) → Fe(II) reduction,[92−95] implying that Fe exists in the form of Fe^{3+} in the β-CD solution. Interestingly, the introduction of β-CD into the $FeCl_3$ solution leads to a significant decrease of the peak current (I, μA) at 193 mV from −60.37 to −48.20 μA, together with a negative shift (−19 mV) of the reduction potential to 174 mV, as shown by a black

dx.doi.org/10.1021/jp303041v | J. Phys. Chem. B 2012, 116, 7635−7643

arrow. These observations are assumed to arise from the interaction between β-CD and Fe^{3+} in the solution during stirring. UV−vis absorption spectra of the solutions of $FeCl_3$ in the absence and presence of β-CD (2.27 g, 2.00×10^{-2} mol·dm^{-3}) show an absorption band at 233 nm with almost the same intensity due to the characteristic absorption band of Fe^{3+} ions.[74] This indicates that the $FeCl_3$ in solution was not changed (hydrolyzed or reduced) with the addition of β-CD.

Taken together, all of these findings demonstrate that the reduction process of $FeCl_3$ to $FeCl_2$ occurs in the carbonization process of β-CD and its degradation products rather than in the degradation process in solution. This not only allows us to consider that $FeCl_3$ may play a role of a catalyst during the degradation reaction of β-CD in solution but also leads us to propose a possible reaction (eq 1) to describe the reduction process at 373 K in air based on XRD and XPS analyses.

$$C + 4FeCl_3 + 2H_2O \xrightarrow{\Delta} 4FeCl_2 + 4HCl\uparrow + CO_2\uparrow \quad (1)$$

More Effective Degradation of β-CD Induced by $FeCl_3$. Thermal analysis is an effective tool to investigate how the thermal property of components is changed by intimate mixing.[96−98] In order to quantitatively evaluate the effect of $FeCl_3$ on the degradation of β-CD, we performed TG and ESI-MS measurements. Figure 8 displays TG profiles of the decomposition process of β-CD, $FeCl_3 \cdot 6H_2O$, and $\mathbf{M_1}$, from which we can obtain information on residual masses (RM, %) at different temperatures.

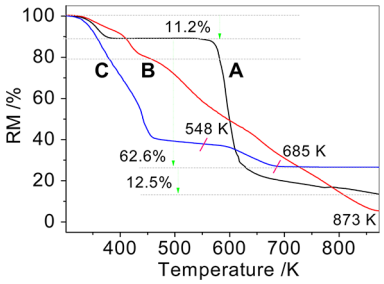

Figure 8. TG profiles of β-CD (A), $\mathbf{M_1}$ (B), and $FeCl_3 \cdot 6H_2O$ (C).

For free $FeCl_3 \cdot 6H_2O$, the mass loss (60.5%) in the range of 324−548 K is due to the release of crystal water and HCl (see eq 2), and the other mass loss (9.9%) from 549 to 685 K is due to the decomposition of $Fe(OH)_3$ (eq 3).[99,100] The decomposition of β-CD is divided in three stages,[101−106] (i) water release of 11.2%, (ii) a sharp mass loss of 62.6% owing to rupture of 1,4-glycosidic bonds and generation of numerous gaseous species, and (iii) a slow carbonization process with a mass loss of 12.5%. However, we notice that curve B in the figure has a completely different profile from curves A and C. The intimate mixture indicates a continuous mass loss over the whole range, without any flat portions. We infer that the $FeCl_2$ that originated from the reduction of $FeCl_3$ may further partially decompose into Fe based on the low RM value (5.4%) of the mixture at 873 K in nitrogen. This supposition is confirmed by the XRD result of Figure 9.

$$FeCl_3 \cdot 6H_2O \xrightarrow{\Delta} Fe(OH)_3 + 3H_2O\uparrow + 3HCl\uparrow \quad 2)$$

$$2Fe(OH)_3 \xrightarrow{\Delta} Fe_2O_3 + 3H_2O \quad 3)$$

As seen in Figure 9, the sintering product of the intimate mixture at 873 K exhibits two sets of main diffraction peaks,

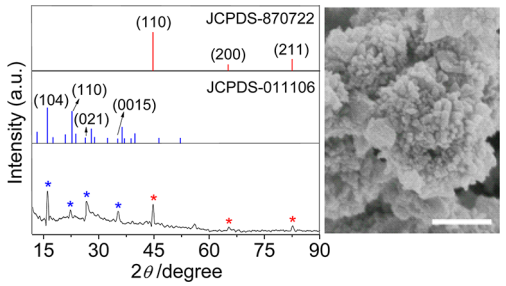

Figure 9. XRD pattern (left) and FE-SEM image (right) of the sintering product of the intimate mixture of β-CD and $FeCl_3$ at 873 K for 15 min under a nitrogen atmosphere. Scale bar = 200 nm.

one set at 16.1, 22.4, 26.6, 35.1, and 39.0° and the other at 44.7, 65.1, and 82.5°, which are indexed to the hexagonal crystal system of $FeCl_2$ (JCPDS 01-1106)[107,108] and the cubic crystal system (JCPDS 87-0722)[109,110] of Fe, respectively. This observation signifies the formation of an in situ composite of Fe and $FeCl_2$ at higher temperature. Equation 4 depicts the decomposition of $FeCl_2$ in nitrogen. The molar ratio of $FeCl_2$ to Fe in the composite material is determined to be 3:1 in light of the XPS analysis.[74] Figure 9 shows that the Fe@$FeCl_2$ composite material looks like a coralline structure, ranging from 50 to 150 nm in diameter.

In order to give a direct comparison in degradation degrees (α) of β-CD between the free state and the intimate mixture, we make a conversion from RM to α, according to eqs 5 (α_1 for curve A) and 6 (α_2 for curve B).

$$FeCl_2 \xrightarrow[\Delta]{N_2} Fe + Cl_2\uparrow \quad 4)$$

$$\alpha_1 = 1 - RM \times (1 - r_1)^{-1} \quad (5)$$

$$\alpha_2 = 1 - (RM - r_2 - r_3) \times (1 - r_1 - r_2 - r_3)^{-1} \quad (6)$$

In the equations, r_1, r_2, and r_3 represent the mass percentages of water, $FeCl_2$, and Fe. r_1 is determined based in Figure 8, and r_2 and r_3 are obtained from the XPS result and the initial content of Fe. For example, at 873 K, the α_1 and α_2 values are 83.5 and 98.8%, respectively. Both an increase of 15.3% in α values and a degradation efficiency of almost 99% provide strong evidence for the significant effect of $FeCl_3$ on the decomposition process of β-CD. Mass spectroscopy data in Figure 10 further substantiates this conclusion.

ESI-MS spectra of the solutions of β-CD after treatment without and with $FeCl_3$ are depicted in Figure 10A and B, respectively, showing a huge difference in the number, position,

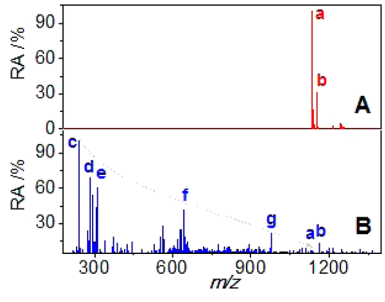

Figure 10. ESI-MS spectra of the solutions (pH 2.0) of β-CD after treatment without (A) and with (B) $FeCl_3$.

dx.doi.org/10.1021/jp303041v | J. Phys. Chem. B 2012, 116, 7635−7643

and relative abundance (RA) of peaks between them. In the case of the free β-CD solution, there are only two strong molecule−ion peaks, one at m/z = 1135 (a, RA 100%) and the other at m/z = 1153 (b, RA 30%), arising from $[\beta\text{-CD}]^+$ and $[\beta\text{-CD}\cdot H_2O]^+$, respectively. However, in the solution of β-CD and $FeCl_3\cdot 6H_2O$, peaks a and b have very low intensity (RA < 15%); instead, numerous signals are observed in the range of 200−1100. It demonstrates that the effect of $FeCl_3$ on the degradation of β-CD is far more outstanding than that of acidity.

Apparently, several main molecule−ion peaks at m/z = 240 (c, $C_8H_{16}O_8^+$, 100%), 282 (d, $C_{11}H_{22}O_8^+$, 65%), 310 (e, $C_{12}H_{22}O_9^+$, 60%), 639 (f, $C_{24}H_{47}O_{19}^+$, 40%), and 978 (g, $C_{36}H_{66}O_{30}^+$, 28%) in Figure 10B are derived from the degradation of β-CD, indicating that the degradation products of β-CD mainly exist in the form of one single glucopyranose unit (c−e), three units (f), and finally five units (g).[74] The occurrence of numeruous fragments with low m/z is indicative of high degradation efficiency. To explain the drastic difference between with and without $FeCl_3$, we propose that an interaction between Fe^{3+} ions and oxygen atoms, probably as well as the interaction between Cl^- ions and hydrogen atoms, facilitates the rupture of 1,4-glycosidic bonds of β-CD. Similar molecule−ion interactions and their effects have been observed in our recent studies by gas chromatography coupled to time-of-flight mass spectrometry.[111−115]

Low-Temperature Carbonization and More Effective Degradation of Amylose Induced by $FeCl_3$. In order to extend these prior observations, we present here the results of a study on the system of amylose and $FeCl_3$. Figure 11 shows XRD patterns and the photographs of $\mathbf{M}_4$ and $\mathbf{M}_5$ as well as free amylose dried at the same conditions (373 K for 2 h).

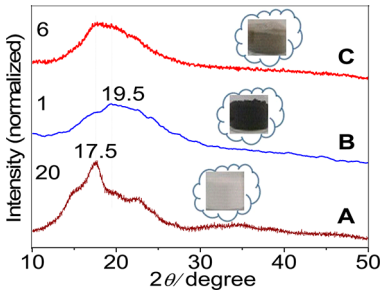

Figure 11. Photographs and XRD patterns of the dried amylose (A), $\mathbf{M}_4$ (B), and $\mathbf{M}_5$ (C). The relative signal intensity was normalized to the intensity of the peak at 17.5° in curve A.

The dried amylose has a strong diffraction peak at a 2θ angle of 17.5°. Nevertheless, it becomes broader in the $\mathbf{M}_5$ but almost disappears in the $\mathbf{M}_4$. Also, there is a strong broad peak centered at 19.5° in the two $\mathbf{M}_4$ series materials. These suggest that the crystallinity of amylose is destroyed largely. In addition, the photographs indicate that the color of the powder becomes progressively deeper from the dried amylose (white) to the $\mathbf{M}_5$ (brown) and to the $\mathbf{M}_4$ (black). What is more, the cellulose yields a similar result as amylose.[74] These findings demonstrate that the presence of $FeCl_3$ exerts a significant impact on the degradation of amylose and cellulose. Two independent experiments (TG/DTG and ESI-MS) reveal the change in the degradation process and degradation products of amylose.

First, a comparison between the TG/DTG profiles of amylose before and after mixing with $FeCl_3$ indicates two striking changes in the presence of $FeCl_3$, a much lower degradation temperature and a complete degradation; see Figure 12. The former is illustrated by green arrows in the

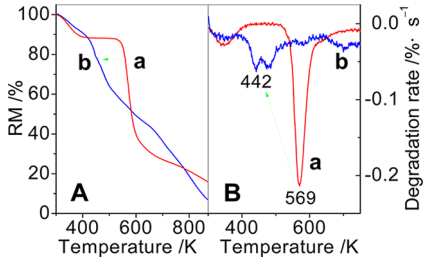

Figure 12. TG (A) and DTG (B) profiles of amylose (a) and $\mathbf{M}_4$ (b).

figure, showing a decrease of 127 K at the maximum degradation temperature. The latter is reflected by large differences in α values. For example, the α values of amylose in the absence and presence of $FeCl_3$ at 873 K are 82.5 and 96.8%, respectively, showing a significant increase of the degradation ($\Delta\alpha$, 14.3%). It is worthy of note that the presence of $FeCl_3$ also causes a decrease (about 65 K) of the maximum degradation temperature of cellulose and a slight increase ($\Delta\alpha$, 3.2%, from 95.5 to 98.7%) in α values of cellulose at 873 K.[74] These changes are a good reflection of the change in the crystallinity of amylose and cellulose induced by an interaction between $FeCl_3$ and them.

Figure 13 shows ESI-MS spectra of the solutions of amylose with and without $FeCl_3$. Obviously, the acidic condition only

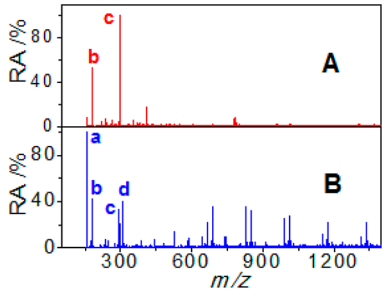

Figure 13. ESI-MS spectra of the solutions of amylose after treatment without (A) and with (B) $FeCl_3$.

results in the degradation of amylose into two main fragment peaks (RA > 20%) at m/z = 179 (b, $C_6H_{11}O_6^+$, 59%) and 295 (c, $C_{11}H_{19}O_9^+$, 100%). However, the addition of $FeCl_3$ causes a large degradation of amylose to produce more fragments with higher RA (12 fragments, RA > 20%), and the two strongest signals appear at m/z = 155 (a, $C_{12}H_{22}O_9^{2+}$, 100%) and 310 (d, $C_{12}H_{22}O_9^+$, 45%). What is more, no high-intensity peak (RA > 50%) is observed except for the small fragment a. These results indicate that the presence of $FeCl_3$ destroys many of the linkage sites between the amylose subunits.[74]

As we know, amylose is a polymer of glucose linked by 1,4-glycosidic bonds, mainly in linear chains. The ESI mass spectrum of amylose under acidic conditions (pH 2.0) indicates that the degradation of amylose is influenced by the acidity only to a small extent because the acidic condition only causes limited cleavage patterns of amylose chains. However, with the addition of $FeCl_3$, more small fragments (a−d) with relatively high abundances, and especially the significant decrease in RA of fragments b and c, are detected, revealing that the presence

dx.doi.org/10.1021/jp303041v | J. Phys. Chem. B 2012, 116, 7635−7643

of $FeCl_3$ leads to a major change in cleavage mechanisms (including cleavage patterns and cleavage sites) of amylose chains.

Further, the change is more noticeable in the case of β-CD, as shown in Figure 10, because $FeCl_3$ results in extensive breakdown of the 1,4-glycosidic linkages in β-CD molecules. This difference in the effect of $FeCl_3$ on the degradation of β-CD and amylose can be related to the structural difference between the sugars, mainly including molecular weight and conformation (a linear chain for amylose and a cyclic structure for β-CD).

We consider that the change induced by $FeCl_3$ is closely associated with the intimate mixing process in solution. That is to say, the more effective degradation of the carbohydrates in solution to generate more small fragments is an important reason for the low-temperature carbonization in the solid state. This can be seen from the fact that the physical mixtures of $FeCl_3$ and the carbohydrates in the solid state were not carbonized at all of the same drying conditions.[74]

Taken together, especially in conjunction with those pictures (Figure 4D and Figure 11C) with regard to the effect of acidity, these results suggest that the formation of more small fragments in ESI mass spectra may be an indication of more effective degradation of carbohydrates. Therefore, we infer that $FeCl_3$ plays a role in promoting the degradation of carbohydrates.

CONCLUSIONS

The present study demonstrates that $FeCl_3$ catalyzes the degradation of β-CD in the solution, leading to the occurrence of carbonization of the mixed β-CD at a much lower temperature (373 K) in air. The carbonization promotion is present even if a small amount of $FeCl_3$ is added. The formation of the $FeCl_2$ crystal at 373 K suggests the reduction of $FeCl_3$ by graphite carbon materials formed during the carbonization of β-CD in air. Interestingly, the Fe@$FeCl_2$ composite material with a coralline nanostructure is formed by sintering the intimate mixture of $FeCl_3$ and β-CD in nitrogen. Further experiments reveal the effect of $FeCl_3$ on the carbonization and degradation of amylose and cellulose. We believe that this work provides new insight into the application of noncovalent interactions between inorganic salts and carbohydrates.

ASSOCIATED CONTENT

Supporting Information

(1) XRD pattern and photograph of the dried β-CD; (2) UV−vis spectra of the solutions of $FeCl_3$ and β-CD; (3) XPS curve of the Fe@$FeCl_2$ composite material; (4) proposed structures of fragments c, d, e, f, and g from the degradation of β-CD and fragments a, b, c, and d from the degradation of amylose; (5) photographs, XRD patterns, and TG/DTG profiles of cellulose samples; and (6) photographs of the physical mixtures of $FeCl_3$ and the carbohydrates in the solid state. This material is available free of charge via the Internet at http://pubs.acs.org.

AUTHOR INFORMATION

Corresponding Author

*Telephone: 86-551-3492002. Fax: 86-551-3601592. E-mail: solexin@ustc.edu.cn.

Notes

The authors declare no competing financial interest.

ACKNOWLEDGMENTS

The authors are grateful to NSFC of China (No. 21071139) for financial support of this work.

REFERENCES

(1) Dincer, I. *Renewable Sustainable Energy Rev.* **2000**, *4*, 157−175.
(2) Malik, S. N.; Sukhera, O. R. *Renewable Sustainable Energy Rev.* **2012**, *16*, 1282−1290.
(3) Ghorashi, A. H.; Rahimi, A. *Renewable Sustainable Energy Rev.* **2011**, *15*, 729−736.
(4) Shen, Y. C.; Chou, C. J.; Lin, G. T. R. *Energy* **2011**, *36*, 2589−2598.
(5) Pan, X. J.; Sano, Y. *Bioresour. Technol.* **2005**, *96*, 1256−1263.
(6) Tamaki, Y.; Mazza, G. *Ind. Crops Prod.* **2010**, *31*, 534−541.
(7) Climent, M. J.; Corma, A.; Iborra, S. *Green Chem.* **2011**, *13*, 520−540.
(8) Seyedia, S. M.; Zohuria, G. H.; Sandaroosa, R. *Supramol. Chem.* **2011**, *23*, 509−517.
(9) Borrega, M.; Nieminen, K.; Sixta, H. *Bioresour. Technol.* **2011**, *102*, 10724−10732.
(10) Wang, X. Y.; Cheng, J. J. *Energy Fuels* **2011**, *25*, 1830−1836.
(11) Kumar, P.; Barrett, D. M.; Delwiche, M. J.; Stroeve, P. *Ind. Eng. Chem. Res.* **2009**, *48*, 3713−3729.
(12) Amidon, T. E.; Wood, C. D.; Shupe, A. M.; Wang, Y.; Graves, M.; Liu, S. J. *J. Biobased Mater. Bio.* **2008**, *2*, 100−120.
(13) Bennetto, H. P.; Delaney, G. M.; Mason, J. R.; Roller, S. D.; Stirling, J. L.; Thurston, C. F. *Biotechnol. Lett.* **1985**, *7*, 699−704.
(14) Redding, A. P.; Wang, Z. Y.; Keshwani, D. R.; Cheng, J. J *Bioresour. Technol.* **2011**, *102*, 1415−1424.
(15) Teske, A.; Durbin, A.; Ziervogel, K.; Cox, C.; Arnosti, C. *Appl. Environ. Microbiol.* **2011**, *77*, 2008−2018.
(16) Cao, X. Y.; Ro, K. S.; Chappell, M.; Li, Y.; Mao, J. D. *Energy Fuels* **2011**, *25*, 388−397.
(17) Iqbal, M. S.; Akbar, J.; Saghir, S.; Karim, A.; Koschella, A.; Heinze, T.; Sher, M. *Carbohydr. Polym.* **2011**, *86*, 1775−1783.
(18) Li, G. Y.; Huang, L. H.; Hse, C. Y.; Qin, T. F. *Carbohydr. Polym.* **2011**, *85*, 560−564.
(19) Kim, D. H.; Wu, J. Y.; Jenog, K. W.; Kim, M. S.; Shin, H. S. *Int. J. Hydrogen Energy* **2011**, *36*, 10666−10673.
(20) Hansen, M. A. T.; Kristensen, J. B.; Felby, C.; Jorgensen, H. *Bioresour. Technol.* **2011**, *102*, 2804−2813.
(21) Correc, G.; Hehemann, J. H.; Czjzek, M.; Helbert, W. *Carbohydr. Polym.* **2011**, *83*, 277−283.
(22) Onwudili, J. A.; Williams, P. T. *Green Chem.* **2011**, *13*, 2837−2843.
(23) Bu, L. T.; Beckham, G. T.; Shirts, M. R.; Nimlos, M. R.; Adeny, W. S.; Himmel, M. E.; Crowley, M. F. *J. Biol. Chem.* **2011**, *20*, 18161−18169.
(24) Berghem, L. E. R.; Pettersson, L. G. *Eur. J. Biochem.* **1973**, *37*, 21−30.
(25) Willats, W. G. T.; Limberg, G.; Buchholt, H. C.; Alebeek, G. J. V.; Benen, J.; Christensen, T. M. I. E.; Visser, J.; Voragen, A.; Mikkelsen, J. D.; Knox, J. P. *Carbohydr. Res.* **2000**, *327*, 309−320.
(26) Vanetten, C. H.; Dacenbichler, M. E.; Peters, J. E.; Tookey, H. L. *J. Agric. Food Chem.* **1966**, *14*, 426−430.
(27) Hocking, P. J.; Marchessault, R. H. *Macromolecules* **1996**, *29*, 2472−2478.
(28) Hubert, C.; Denicourt-Nowicki, A.; Roucoux, A.; Landy, D.; Leger, B.; Crowyn, G.; Monflier, E. *Chem. Commun.* **2009**, 1228−1230.
(29) Tran, D. N.; Legrand, F. X.; Menuel, S.; Bricout, H.; Tilloy, S.; Monflier, E. *Chem. Commun.* **2012**, *48*, 753−755.
(30) Caron, L.; Bricout, H.; Tilloy, S.; Ponchel, A.; Landy, D.; Fourmentin, S.; Monflier, E. *Adv. Synth. Catal.* **2004**, *346*, 1449−1456.
(31) Song, L. X.; Bai, L. *J. Phys. Chem. B* **2009**, *113*, 11724−11731.
(32) Song, L. X.; Wang, H. M.; Guo, X. Q.; Bai, L. *J. Org. Chem.* **2008**, *73*, 8305−8316.

(33) Yang, Y. W.; Chen, Y.; Liu, Y. *Inorg. Chem.* **2006**, *45*, 3014−3022.
(34) Hasegawa, Y.; Inoue, Y.; Deguchi, K.; Ohki, S.; Tansho, M.; Shimizu, T.; Yazawa, K. *J. Phys. Chem. B* **2012**, *116*, 1758−1764.
(35) Chao, J. B.; Su, J.; Li, J. X.; Zhao, W.; Huang, S. P.; Du, R. *Supramol. Chem.* **2011**, *23*, 644−653.
(36) Braga, S. S.; Gago, S.; Seixas, J. D.; Valente, A. A.; Pillinger, M.; Santos, T. M.; Goncalves, I. S.; Romao, C. C. *Inorg. Chim. Acta* **2006**, *359*, 4757−4764.
(37) Swiech, O.; Mieczkowska, A.; Chmurski, K.; Bilewicz, R. *J. Phys. Chem. B* **2012**, *116*, 1765−1771.
(38) Liu, Y.; Zhao, Y. L.; Zhang, H. Y.; Song, H. B. *Angew. Chem.* **2003**, *115*, 3382−3385.
(39) Wang, H. M.; Song, L. X. *Chem. Lett.* **2007**, *136*, 596−597.
(40) Liu, Y.; Wang, H.; Liang, P.; Zhang, H. Y. *Angew. Chem.* **2004**, *116*, 2744−2748.
(41) Chen, Y.; Zhang, Y. M.; Liu, Y. *Chem. Commun.* **2010**, *46*, 5622−5633.
(42) Riela, S.; Lazzara, G.; Meo, P. L.; Guernelli, S.; D'Anna, F.; Milioto, S.; Noto, R. *Supramol. Chem.* **2011**, *23*, 819−828.
(43) Song, L. X.; Bai, L. *J. Phys. Chem. B* **2009**, *113*, 9035−9040.
(44) Bai, L.; Song, L. X.; Wang, M.; Zhu, L. H. *Chin. J. Chem. Phys.* **2010**, *23*, 117−124.
(45) Yang, J.; Song, L. X.; Yang, J.; Dang, Z.; Chen, J. *Dalton Trans.* **2012**, *41*, 2393−2398.
(46) Song, L. X.; Pan, S. Z.; Bai, L.; Dang, Z.; Du, F. Y.; Chen, J. *Supramol. Chem.* **2011**, *23*, 447−454.
(47) Song, L. X.; Wang, M.; Dang, Z.; Du, F. Y. *J. Phys. Chem. B* **2010**, *114*, 3404−3410.
(48) Song, L. X.; Wang, H. M.; Yang, Y. *Bull. Chem. Soc. Jpn.* **2007**, *80*, 2185−2195.
(49) Song, L. X.; Yang, J.; Bai, L.; Du, F. Y.; Chen, J.; Wang, M. *Inorg. Chem.* **2011**, *50*, 1682−1688.
(50) Saskia, A. G.; Michale, J. B.; Engberts, J. B. F. N. *J. Am. Chem. Soc.* **1990**, *112*, 9665−9666.
(51) Ingram, L. J.; Taylor, S. D. *Angew. Chem., Int. Ed.* **2006**, *19*, 3503−3506.
(52) Werz, D. B.; Ranzinger, R.; Herget, S.; Adibekian, A.; Lieth, C. W. V. D.; Seeberger, P. H. *ACS Chem. Biol.* **2007**, *2*, 685−691.
(53) Vyas, M. N.; Vyas, N.; Quiocho, F. *Biochemistry* **1994**, *33*, 4762−4768.
(54) Li, Y.; Chen, J. F.; Xu, Q.; He, L. H.; Chen, Z. M. *J. Phys. Chem. C* **2009**, *113*, 10085−10089.
(55) Liu, C. L.; Dong, W. S.; Song, J. R.; Liu, L. *Mater. Sci. Eng., A* **2007**, *459*, 347−354.
(56) Veiga, M. D.; Merino, M. *J. Pharm. Biomed. Anal.* **2002**, *28*, 973−982.
(57) Rosa, C. D. *Macromolecules* **1997**, *30*, 5494−5500.
(58) Tzeng, S. S.; Chr, Y. G. *Mater. Chem. Phys.* **2002**, *73*, 162−169.
(59) Chen, Y. J.; Chen, J.; Zeng, C. L. *J. Power Sources* **2010**, *195*, 1914−1919.
(60) Bertoluzza, A.; Rossi, M.; Taddei, P.; Redenti, E.; Zanol, M.; Ventura, P. *J. Mol. Struct.* **1999**, *480*−*481*, 535−539.
(61) Sone, T.; D'Amato, R.; Mawatari, Y.; Tabata, M.; Furlani, A.; Russo, M. V. *J. Polym. Sci., Part A: Polym. Chem.* **2004**, *42*, 2365−2376.
(62) Kudin, K. N.; Ozbas, B.; Schniepp, H. C.; Prud'homme, R. K.; Aksay, I. A.; Car, R. *Nano Lett.* **2008**, *8*, 36−41.
(63) Nemanich, R. J.; Solin, S. A. *Phys. Rev. B* **1979**, *20*, 392−401.
(64) Calizo, I.; Balandin, A. A.; Bao, W.; Miao, F.; Lau, C. N. *Nano Lett.* **2007**, *7*, 2645−2649.
(65) Tommasini, M.; Castiglioni, C.; Zerbi, G. *Phys. Chem. Chem. Phys.* **2009**, *11*, 10185−10194.
(66) Graf, D.; Molitor, F.; Ensslin, K.; Stampfer, C.; Jungen, A.; Hierold, C.; Wirtz, L. *Nano Lett.* **2007**, *7*, 238−242.
(67) Castiglioni, C.; Negri, F.; Rigolio, M.; Zerbi, G. *J. Chem. Phys.* **2001**, *115*, 3769−3778.
(68) Song, L. X.; Xu, P. *J. Phys. Chem. A* **2008**, *112*, 11341−11348.
(69) Huang, L.; Allen, E.; Tonelli, A. E. *Polymer* **1999**, *40*, 3211−3221.
(70) Sun, X. F.; Sun, R. C.; Sun, J. X. *Bioresour. Technol.* **2004**, *95*, 343−350.
(71) Bourdillon, C.; Bourgeois, J. P.; Thomas, D. *J. Am. Chem. Soc.* **1980**, *102*, 4231−4235.
(72) Ali, H. A.; Iliadis, A. A.; Mulligan, R. F.; Cresce, A. V. W.; Kofinas, P.; Lee, U. *Solid-State Electron.* **2002**, *46*, 1639−1642.
(73) Mansur, H. S.; Sadahira, C. M.; Souza, A. N.; Mansur, A. A. P. *Mater. Sci. Eng., C* **2008**, *28*, 539−548.
(74) See the Supporting Information.
(75) Song, L. X.; Pan, S. Z.; Zhu, L. H.; Wang, M.; Du, F. Y.; Chen, J. *Inorg. Chem.* **2011**, *50*, 2215−2223.
(76) Song, L. X.; Chen, J.; Zhu, L. H.; Xia, J.; Yang, J. *Inorg. Chem.* **2011**, *50*, 7988−7996.
(77) Dang, Z.; Song, L. X.; Yang, J.; Chen, J.; Teng, Y. *Dalton Trans.* **2012**, *41*, 3006−3013.
(78) Martin Dei Valle, E. M. *Process Biochem.* **2004**, *39*, 1033−1046.
(79) George, C.; Kuriakose, S.; Georgea, S.; Mathewb, T. *Supramol. Chem.* **2011**, *23*, 593−597.
(80) Szejtli, J. *Chem. Rev.* **1998**, *98*, 1743−1754.
(81) Haider, J. M.; Pikramenou, Z. *Chem. Soc. Rev.* **2005**, *34*, 120−132.
(82) Zheng, W. X.; Tarr, M. A. *J. Phys. Chem. B* **2004**, *108*, 10172−10176.
(83) Narumi, Y.; Katsumata, K.; Nakamura, T.; Tanaka, Y.; Shimomura, S; Ishikawa, T; Yabashi, M. *J. Phys.: Condens. Matter* **2004**, *16*, LS7−L63.
(84) Norbert, L.; Bjorn, K. *J. Phys. Chem. B* **2008**, *112*, 12374−12385.
(85) Aee, Y. J.; Lee, J. W.; Bae, C. J.; Park, J. G.; Noh, H. J.; Park, J. H.; Hyeno, T. *Adv. Funct. Mater.* **2005**, *15*, 503−509.
(86) Prozorov, T.; Mallapragada, S. K.; Narasimhan, B.; Wang, L. J.; Palo, P.; Nilsen-Hamilton, M.; Williams, T. J.; Bazylinski, D. A.; Prozorov, R.; Canfield, P. C. *Adv. Funct. Mater.* **2007**, *17*, 951−957.
(87) Russo, M. V.; Polzonetti, G.; Furlani, A. *Synth. Met.* **1991**, *39*, 291−301.
(88) Zhang, Y.; Zhang, Z. X.; Li, T. B.; Liu, X. G.; Xu, B. S. *Spectrochim. Acta, Part A* **2008**, *70*, 1060−1064.
(89) Lin, Y. X.; Cai, W. P.; Tian, X. Y.; Liu, X. L.; Wang, G. Z.; Liang, C. H. *J. Mater. Chem.* **2011**, *21*, 991−997.
(90) Nagarajan, N.; Zhitomirsky, I. *J. Appl. Electrochem.* **2006**, *36*, 1399−1405.
(91) Grosvenor, A. P.; Kobe1, B. A.; Biesinger1, M. C.; Mcintyre, N. S. *Surf. Interface Anal.* **2004**, *36*, 1564−1574.
(92) Patra, R.; Chaudhary, A.; Ghosh, S. K.; Rath, S. P. *Inorg. Chem.* **2008**, *47*, 8324−8335.
(93) Patolsky, F.; Zayats, M.; Katz, E.; Willner, I. *Anal. Chem.* **1999**, *71*, 3171−3180.
(94) Yomathan, J. N.; Wood, K. S.; Meyer, T. J. *Inorg. Chem.* **1993**, *31*, 3280−3285.
(95) Pye, S.; Winnick, J.; Kohl, P. A. *J. Electrochem. Soc.* **1997**, *144*, 1934−1938.
(96) Song, L. X.; Wang, M.; Pan, S. Z.; Yang, J.; Chen, J.; Yang, J. *J. Mater. Chem.* **2011**, *21*, 7982−7989.
(97) Song, L. X.; Xia, J.; Dang, Z.; Wang, L. B.; Chen, J.; Yang, J. *CrystEngComm* **2012**, *14*, 2675−2682.
(98) Chen, J.; Song, L. X.; Yang, J.; Xia, J.; Shao, Z. C. *J. Mater. Chem.* **2012**, *41*, 6251−6258.
(99) Twidwell, L. G.; Thompson, R. J. *J. Mineral.* **2001**, *53*, 15−17.
(100) Zhu, X. J.; Zhu, Y. W.; Murali, S.; Stoller, M. D.; Ruoff, R. S. *ACS Nano* **2011**, *5*, 3333−3338.
(101) Song, L. X.; Du, F. Y.; Yang, J.; Dang, Z.; Yang, J.; Shao, Z. C. *Soft Matter* **2011**, *7*, 6671−6677.
(102) Pan, S. Z.; Song, L. X.; Chen, J.; Du, F. Y.; Yang, J.; Xia, J. *Dalton Trans.* **2011**, *40*, 10117−10124.
(103) Song, L. X.; Teng, C. F.; Yang, Y. *Inclusion Phenom. Macrocyclic Chem.* **2006**, *54*, 221−232.
(104) Xu, P.; Song, L. X.; Wang, H. M. *Thermochim. Acta* **2008**, *469*, 36−42.
(105) Song, L. X.; Wang, H. M.; Xu, P.; Zhang, Z. Q. *Bull. Chem. Soc. Jpn.* **2007**, *80*, 2313−2322.

(106) Song, L. X.; Du, F. Y.; Guo, X. Q.; Pan, S. Z. *J. Phys. Chem. B* **2010**, *114*, 1738−1744.
(107) Vaira, M. D.; Midollini, S.; Sacconi, L. *Inorg. Chem.* **1981**, *20*, 3430−3435.
(108) Herber, H. R.; Nowik, I.; Kostner, M. E.; Kahlenberg, V.; Kreutz, C.; Laus, G.; Schottenberger, H. *Int. J. Mol. Sci.* **2011**, *12*, 6397−6406.
(109) Uddin, M. N.; Yang, Y. S. *J. Mater. Chem.* **2009**, *19*, 2909−2911.
(110) Guo, X. W.; Fang, X. P.; Mao, Y.; Wang, Z. X.; Wu, F.; Chen, L. Q. *J. Phys. Chem. C* **2011**, *115*, 3803−3808.
(111) Guo, X. Q.; Song, L. X.; Du, F. Y.; Dang, Z.; Wang., M. *J. Phys. Chem. B* **2011**, *115*, 1139−1144.
(112) Du, F. Y.; Song, L. X.; Wang, M.; Pan, S. Z.; Zhu, L. H.; Yang, J. *Soft Matter* **2011**, *7*, 9078−9083.
(113) Yang, J.; Song, L. X.; Dang, Z.; Pan, S. Z.; Du, F. Y. *Chin. Chem. Lett.* **2011**, *22*, 1347−1350.
(114) Wang, M.; Song, L. X.; Dang, Z.; Zhu, L. H.; Yang, J. *Chem. Lett.* **2011**, *40*, 478−479.
(115) Song, L. X.; Dang, Z. *J. Phys. Chem. B* **2009**, *113*, 4998−5000.